# Photoinduced Electron Transfer on the Surfaces of Micelles

**Kristin Weidemaier, H. L. Tavernier, and M. D. Fayer***

*Department of Chemistry, Stanford University, Stanford, California 94305*

*Received: July 10, 1997; In Final Form: September 4, 1997*[⊗]

Photoinduced electron transfer between *N*,*N*-dimethylaniline (DMA) and octadecylrhodamine B (ODRB) is studied on the surfaces of three alkyltrimethylammonium bromide micelles: dodecyl- (DTAB), tetradecyl- (TTAB), and hexadecyltrimethylammonium bromide (CTAB). The DMA and ODRB molecules are localized at the micelle surface. Time-resolved fluorescence and fluorescence yield data are presented and analyzed with the theoretical methods of ref 1. Lateral diffusion of the molecules over the micelle surfaces is included. Although the three micelles are structurally similar, pronounced differences in the electron-transfer kinetics are observed, with the overall amount of electron transfer increasing with alkyl chain length for the same DMA surface packing fraction. This result is attributed to differences in the solvent reorganization energy, possibly due to varying extents of water penetration into the headgroup regions of the three micelles. As the surfactant chain length increases, the solvent reorganization energy is reduced, resulting in faster electron transfer.

## I. Introduction

There is currently a great deal of interest in electron-transfer dynamics in micelle systems.[1−9] The goals of research on such systems are 2-fold. The first is to obtain a fundamental understanding of how system geometry impacts the reaction dynamics, and the second is to develop techniques for designing efficient charge-separating systems. In pursuing the latter goal, advantage can be taken of phase separation between the micelle and water to promote ion survival.[4,10−13] The results of previous studies provide an impetus for detailed theoretical and physical understanding of the electron-transfer dynamics.

Developing an understanding of electron transfer in restricted geometries such as micelles is a complex problem. For reactions at micelle surfaces involving multiple donors or acceptors, any one of which can participate in the transfer process, a theory is needed to account for all possible electron-transfer pathways, with the diffusion of the molecules included and the spatial averages properly performed. The form of the distance-dependent electron-transfer rate coefficient must also be known. It is only with the aid of an appropriate theoretical model that the effects of diffusion can be separated from those due to the form of the transfer rate itself, so that the various factors contributing to the observed dynamics can be dissected and analyzed. The transfer process involves unanswered questions, such as the role of the solvent in an inhomogeneous system. The nature of the micelle may be important in determining electron-transfer dynamics, and micelle structure and dynamics are active fields of research. Issues such as the depth of water penetration into the micelle, the local viscosity, and diffusion properties will come into play in the description of electron transfer.

Recently, a statistical mechanical theory of photoinduced electron transfer and geminate recombination among donors and acceptors on the surface of a spherical micelle was developed.[1] The donors and acceptors were assumed to be adsorbed close to the surface so that they could be modeled as particles on the surface of a sphere, with their primary motion being lateral diffusion over the micelle surface. (See Figure 1A.) Lateral diffusion rates in micelles and liquid crystalline phases have been measured by $^{13}C$ NMR and were found to range between 2 and 20 Å$^2$/ns.[7,14−16] Theoretical calculations demonstrated that diffusion constants in this range lead to significant enhancement of the amount of electron transfer compared to donors and acceptors that are in random fixed positions on the micelle surface.[1] These results were confirmed by Monte Carlo simulations.[1]

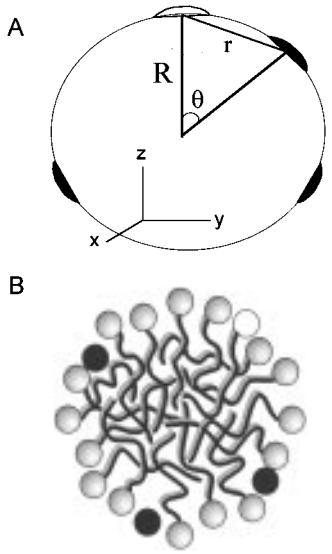


**Figure 1.** (A) Schematic illustrating the model system. The micelle is modeled as a sphere of radius *R*, with the acceptor/donors assumed to be curved disks on the surface. The relevant electron-transfer distance is taken to be *r*, the through-sphere (chord) distance. In the illustration, the unfilled disk denotes the ODRB (no more than one per micelle), while the filled disks are the DMA. (B) A more realistic illustration of an alkyltrimethylammonium bromide micelle with one ODRB (white ball with tail) and several DMAs (black balls).

Although modeling electron transfer at micelle surfaces as that of transfer on a spherical surface is clearly a first approximation to the complicated spatial structure and dynamics of real micelles, this approximation may, nevertheless, be quite reasonable for a variety of micelles. In particular, long-chain ($C_{12}$−$C_{16}$) alkyl surfactants with small ionic headgroups and low aggregation numbers, such as the alkyltrimethylammonium halides, form nearly spherical structures at low concentrations.[17]

[⊗] Abstract published in *Advance ACS Abstracts,* October 15, 1997.

S1089-5647(97)02245-1 CCC: $14.00 

Furthermore, current models of micelles divide the micelle into a dense, liquidlike hydrocarbon interior with little water penetration and a shell approximately 4 Å thick consisting of the polar headgroups, a small amount of hydrocarbon, counterions, and significant amounts of water. Outside of this is bulk water. (See Figure 1B.) NMR studies have distinguished between micelle-bound hydrophobic molecules such as isopropylbenzene, cyclohexane, and pyrene, which tend to be located inside the hydrophobic core, and other molecules such as benzene, nitrobenzene, and *N*,*N*-dimethylaniline, which are preferentially located at the micelle/water interface.[18,19] For molecules of this second type, electron transfer on a spherical surface is a reasonable first approximation.

In this paper we present time-resolved fluorescence and fluorescence yield data for forward electron transfer between *N*,*N*-dimethylaniline (DMA) and octadecylrhodamine B (ODRB) on the surfaces of three alkyltrimethylammonium bromide micelles. As discussed below, both molecules reside near the hydrocarbon/water interface, and thus the electron-transfer dynamics can be modeled by transfer on a spherical surface. The theoretical methods of ref 1 can be used to describe and analyze the dynamics. Because the three surfactants differ only in their hydrocarbon chain length, the properties of the micelles are similar, with the DMA and ODRB localized in similar environments on all micelles. Any differences in electron transfer dynamics should then arise primarily from differences in the micelle sizes, thus providing a good test of the theory. By focusing on a well-defined system, we can subject the data to a careful theoretical examination that will enable the role of diffusion to be understood and the nature of the distance-dependent transfer rate to be examined.

## II. Model and Theory

The model electron-transfer/micelle system has been described previously.[1,20] The micelle is taken to be a sphere of radius *R*. The donor and acceptor molecules are constrained to lie at this radius but can diffuse laterally over the micelle surface. There is at most one molecule that can be photoexcited (electron donor or hole donor) per micelle but no limit to the number of electron acceptors or hole acceptors. Thus, the theory describes the situation for one photoexcited donor and *N* acceptors or, as is the case here, one photoexcited electron acceptor (hole donor) (ODRB) and *N* electron donors (hole acceptors) (DMA) per micelle. The micelle concentration is kept low, and the ODRB concentration is even lower so that Förster energy transfer can be neglected and so that electron transfer from a donor on one micelle to an acceptor on another does not occur. Consistent with experimental results, diffusion of the micelles themselves is insignificant on the time scale of the electron-transfer dynamics. Lateral diffusion of the donor and acceptor molecules over the micelle surface is included and expected to be significant.[1,7,14−16]

Since each micelle will have a different configuration of acceptor/donors distributed over the surface, calculation of the observed electron-transfer dynamics requires performing the ensemble average with the lateral diffusion of the molecules appropriately included. Details of the theory were given in ref 1. In particular, we wish to calculate the physical observable $\langle P_{ex}(t)\rangle$, the probability that the ODRB is still excited at time *t*. Photoexcitation with a short laser pulse occurs at time $t = 0$, initiating the transfer dynamics. The brackets, $\langle\ \rangle$, denote an ensemble-averaged probability.

The starting point of the derivation is writing the differential equations for the special case of one donor and one acceptor. For the forward transfer, we can write a differential equation for the Green's function $G_{ex}(\theta,t|\theta_0)$ along with the associated initial and (reflecting) boundary conditions.

$$\frac{\partial}{\partial t}G_{ex}(\theta,t|\theta_0) = D\nabla_\theta{}^2 G_{ex}(\theta,t|\theta_0) - k_f(\theta)\, G_{ex}(\theta,t|\theta_0)$$

$$G_{ex}(\theta,0|\theta_0) = \frac{\delta(\theta-\theta_0)}{2\pi R^2 \sin\theta_0} \qquad (1)$$

$$2\pi R^2 \sin\theta_c D\frac{\partial}{\partial\theta}G_{ex}(\theta,t|\theta_0)|_{\theta=\theta_c} = 0$$

$G_{ex}(\theta,t|\theta_0)$ is the probability per unit surface area of finding the ODRB excited at time *t* with the DMA a distance $\theta$ away, given that the DMA was located at $\theta_0$ at time 0. (Note that the relevant coordinate for the micelle problem is $\theta$, since this completely defines the donor−acceptor separation distance. See Figure 1A.) $\theta_c$ is the donor−acceptor contact distance in angular units. The diffusion operator is

$$D\nabla_\theta{}^2 = \frac{D}{R^2 \sin\theta}\frac{\partial}{\partial\theta}\left[\sin\theta\frac{\partial}{\partial\theta}\right] \qquad (2)$$

where *R* is the micelle radius. Because the donor−acceptor separation distance is completely defined by $\theta$, the diffusion is one-dimensional, and only the polar-angle component of the Laplacian is required. The distance dependence of the rate coefficient, $k_f(\theta)$, can be of any form, including the well-known Marcus expression.[21,22] The transfer rate is taken to depend on the through-sphere (chord length) distance *r*. However, the rate coefficient is expressed in terms of the angular donor−acceptor separation distance, $\theta$, for consistency with eq 1. The two quantities are related by $r = 2R\sin(\theta/2)$. (For the relatively short distances involved in electron transfer, the difference between the cord length and the arc length is small.)

When all *N* acceptors are present, the excited-state survival probability density for a given initial and final configuration, $P_{ex}(\theta_1...\theta_N,t|\theta_{01}...\theta_{0N})$, is given by

$$P_{ex}(\theta_1...\theta_N,t|\theta_{01}...\theta_{0N}) = \prod_{i=1}^{N} G_{ex}(\theta_i,t|_{0i})$$

$P_{ex}(\theta_1...\theta_N,t|\theta_{01}...\theta_{0N})$ is the probability per unit surface area that the donor is still excited at time *t* and the acceptors are at $\theta_1...\theta_N$, given that the *N* acceptors were at $\theta_{01}...\theta_{0N}$ at time $t = 0$. The ensemble-averaged quantity $\langle P_{ex}(t)\rangle_N$ gives the experimentally observed probability of finding the donor excited at time *t*:

$$\langle P_{ex}(t)\rangle_N = \int_{\theta_1}...\int_{\theta_N}\int_{\theta_{01}}...\int_{\theta_{0N}} P_{ex}(\theta_1...\theta_N,t|\theta_{01}...\theta_{0N})2\pi R^2 \times \sin\theta_1...2\pi R^2 \sin\theta_N\, d\theta_1...d\theta_N \frac{\sin\theta_{01}}{2}...\frac{\sin\theta_{0N}}{2}d\theta_{01}...d\theta_{0N} \qquad (3)$$

$$= \left[\int_\theta\int_{\theta_0} G_{ex}(\theta,t|\theta_0)\pi R^2 \sin\theta \sin\theta_0\, d\theta\, d\theta_0\right]^N$$

We now define the joint probability density:

$$S_{ex}(\theta,t) \equiv \int_{\theta_0} G_{ex}(\theta,t|\theta_0)\frac{\sin\theta_0}{2}d\theta_0$$

$S_{ex}(\theta,t)$ is the probability per unit area that the donor is excited at time *t* and the acceptor is at $\theta$ for the one-donor/one-acceptor problem. From eq 3, we see

$$\langle P_{ex}(t)\rangle_N = [\int_{\theta_c}^{\pi} S_{ex}(\theta,t) 2\pi R^2 \sin\theta \, d\theta]^N \quad (4)$$

Using the definition of $S_{ex}(\theta,t)$, one can show that $S_{ex}(\theta,t)$ satisfies the differential equation

$$\frac{\partial}{\partial t} S_{ex}(\theta,t) = D\nabla_\theta^2 S_{ex}(\theta,t) - k_f(\theta)\, S_{ex}(\theta,t)$$

$$S_{ex}(\theta,0) = \frac{1}{4\pi R^2} \quad (5)$$

$$2\pi R^2 \sin\theta_c D \frac{\partial}{\partial\theta} S_{ex}(\theta,t)|_{\theta=\theta_c} = 0$$

Note that in a restricted geometry problem of this type, the number of acceptors $N$ is finite, and the thermodynamic limit cannot be taken. Equations 5 for $S_{ex}(\theta,t)$ cannot be solved analytically, and numerical evaluation must be followed by numerical integration as indicated by eq 4, to give $\langle P_{ex}(t)\rangle_N$.

Equation 4 gives $\langle P_{ex}(t)\rangle_N$ for 1 ODRB and $N$ DMA per micelle surface. (Micelles without any ODRB will not contribute to the experimentally observed signal.) In an experiment, the number of DMA per micelle is assumed to follow a Poisson distribution about the mean $N$. Thus, the actual experimental observable is

$$\langle P_{ex}(t)\rangle = e^{-t/\tau} \sum_{n=0}^{\infty} \frac{e^{-N} N^n}{n!} \langle P_{ex}(t)\rangle_n \quad (6)$$

In eq 6 the term $e^{-t/\tau}$ has been included to account for the ODRB fluorescence decay. $\tau$ is the excited-state lifetime in the absence of electron transfer.

Donor−acceptor excluded volume is included by a short-distance cutoff in the spatial integrals so that the donor and acceptor cannot approach closer than their contact distance, $\theta_c$. There is another type of excluded volume due to the inability of the $N$ DMA molecules to overlap. Spatial configurations that would result in overlap of the DMA molecules need to be excluded from the ensemble average. In the theory presented here, this second type of excluded volume is neglected. However, for fractional occupancies of <5%, this type of excluded volume has been shown to be insignificant[20] and should be negligible for all experimental DMA concentrations used here. Donor−acceptor excluded volume, on the other hand, is significant at all concentrations since it excludes the short distances that have the greatest impact on the electron-transfer dynamics.

Time-resolved fluorescence measurements that monitor the ODRB excited-state population can be directly compared to eq 6. Additional information about the transfer dynamics is obtained from fluorescence yield experiments. The fluorescence yield, $\phi$, is the ratio of the total steady-state fluorescence for a sample containing DMA to that of a sample consisting only of ODRB.

$$\Phi = \frac{\int_0^{\infty} \langle P_{ex}(t)\rangle dt}{\tau} \quad (7)$$

Fits to time-resolved data using eq 6 must yield parameters such that the calculated short-time dynamics, which are obscured by the instrument time resolution, results in eq 7 giving good agreement with the experimental yield data.

## III. Experimental System

We have studied forward electron transfer between *N*,*N*-dimethylaniline (DMA) and photoexcited octadecylrhodamine B (ODRB) on the surfaces of three micelles: dodecyltrimethylammonium bromide (DTAB), tetradecyltrimethylammonium bromide (TTAB), and hexadecyltrimethylammonium bromide (CTAB). ODRB was purchased from Molecular Probes and used without further purification. DMA, TTAB, and DTAB were the highest commercial grade available from Aldrich, while CTAB was from Fluka (99+%). For all three micelles we chose a surfactant concentration, [S], to give a micelle concentration, [M], of 206 $\mu$M. The micelle concentration is related to that of the surfactant by

$$[M] = \frac{[S] - cmc}{N_{agg}}$$

where cmc denotes the critical micelle concentration and $N_{agg}$ the aggregation number. Values of these parameters for each micelle are given in Table 1. The ODRB concentration was 20 $\mu$M, a factor of 10 less than that of the micelles. Four DMA concentrations, all less than 6 mM, were examined for each micelle system. Concentrations less than 6 mM give rise to significant amounts of electron transfer due to the spatial clustering that occurs when acceptor/donors are confined to a micelle.

**TABLE 1: Table of Critical Micelle Concentrations (cmc), Aggregation Numbers ($N_{agg}$), and Micelle Radii ($R$). The radii Were Taken as That of the Hydrocarbon Core and Calculated from the Tanford Equation[26]**

| | cmc (mM)[51] | $N_{agg}$[51] | $R$ (Å) |
|---|---|---|---|
| DTAB | 15 | 50 | 16.7 |
| TTAB | 3.5 | 67 | 19.2 |
| CTAB | 0.8 | 92 | 21.7 |

Because of the small headgroup size and low aggregation number, all three micelles should be spherical and nearly monodisperse at the experimental concentrations.[17,23] At higher surfactant concentrations, CTAB becomes rodlike; however, cryotransmission electron microscopy[24,25] and small-angle X-ray scattering[23] indicate that CTAB is spherical at low concentrations such as those used here.

Since DMA resides preferentially at the edge of the micelle hydrocarbon core (see below), the micelle radii were taken to be those of the core. The radii of the hydrocarbon cores of the three micelles were calculated by the methods of Tanford.[26] (See Table 1.) The molecular radii of DMA and the ODRB headgroup were obtained from molecular modeling and from crystallographic data on similar compounds. The resulting values are 3.05 and 4.45 Å, respectively. The ODRB excited-state lifetime in the absence of electron transfer was measured to be 1.8 ns on all three micelles.

Localization of the acceptor/donors at the core/water interface is justified as follows. For ODRB, studies of fluorescence anisotropy decays indicate that this molecule has negligible affinity for the aqueous phase but exists bound to the micelle with its headgroup at the micelle surface.[27] This is consistent with what would be expected for a molecule with a long ($C_{18}$) hydrocarbon tail and positively charged headgroup.

Determining the DMA position is substantially more difficult. We based our choice of this molecule on the NMR data of Eriksson and Gillberg.[18] Chemical shift measurements of CTAB protons show a large shift of N-CH and α-CH protons upon addition of even small amounts of DMA. Such a shift is consistent with localization of an aromatic ring near these protons. Further addition of DMA leads to a continued shift of the outermost (α-C and N-C) protons until a DMA concentration of 0.7 times the CTAB concentration, when the deeper hydrocarbon protons near the micelle interior begin to show

substantial shift. This is interpreted as due to penetration of DMA into the micelle occurring at very high DMA concentrations after saturation of the surface region.[18]

To further confirm the localization of the DMA at the hydrocarbon/aqueous interface, we have carefully studied the fluorescence spectrum of DMA in the three micelles and in a variety of solvents. The DMA fluorescence shows a pronounced red shift as the solvent becomes more polar. The spectra of DMA in the three micelles is 20 nm to the red of the DMA spectrum in cyclohexane. If some of the DMA were bound deep in the micelle core, we would expect to see a red shoulder on the DMA fluorescence peak in the micelle solutions. The absence of this shoulder indicates that the DMA spends the vast majority of its time near an aqueouslike environment such as would be found at the micelle surface, consistent with the NMR results. If DMA were moving in the micelle interior in such a way as to be frequently sampling an aqueouslike environment, the time scale of this sampling would have to be fast enough that the peaks at the hydrocarbon wavelength and waterlike wavelength would merge into a peak at the average frequency. For the observed 20 nm peak difference, the sampling time would have to be on the order of femtoseconds, which seems unreasonable. Thus, from the fluorescence spectra and the NMR results we conclude that DMA is located in the headgroup region, not in the hydrocarbon core.

It is more difficult to rule out a small amount of DMA being in the aqueous phase, since the frequency difference between the DMA fluorescence peak in the micelles versus the peak in water is significantly smaller than that between the micelle and cyclohexane. However, the NMR results of Eriksson and Gillberg indicate that the DMA is preferentially solubilized at the edge of the hydrocarbon core.[18] Furthermore, if large quantities of DMA were freely dissolved in the water, then at the DMA concentrations used in this experiment ($<$6 mM) no electron transfer would be observed. Only the clustering of DMA near the acceptor caused by adsorption onto the micelle can explain the fast electron-transfer dynamics observed here. This issue will be taken up again in section V.

From the DMA fluorescence spectra, an estimate of the local dielectric constant at the micelle surface (by "surface" we mean the headgroup region) can be made. By comparing the DMA fluorescence spectra in a variety of solvents with that in the three micelles, we place $\epsilon_s$ in the range of 37 (acetonitrile) to 78 (water) for all three micelles. Finally, from fluorescence spectra of ODRB/DMA experimental samples we conclude that no exciplex formation occurs and that quenching of the ODRB fluorescence is via intermolecular (through-solvent) electron transfer.

The free energy of electron transfer, which is necessary in the specific form of the rate coefficient used later, was calculated from[28]

$$\Delta G = \Delta E - h\nu$$

where $h$ is Planck's constant and $\nu$ is the frequency at which the normalized absorption and fluorescence spectra overlap (579 nm).[29] $\Delta E$ is the difference between the donor reduction potential and the acceptor oxidation potential. $\Delta E$ was determined by cyclic voltammetry for rhodamine B (1 mM) and DMA (40 mM) in acetonitrile. Acetonitrile was chosen because its dielectric constant approximates that of the micelle headgroup region. Experiments were performed using a Bioanalytical Systems 10 $\mu$m diameter Pt ultramicroelectrode and an Ensman 400 dual-electrode potentiostat in two-electrode mode. The reference electrode was a silver wire. Redox potentials were measured for donors and acceptors simultaneously, dissolved in one solution so that $\Delta E$ could be obtained directly. Tetrahexylammonium perchlorate (Fluka, 0.1 M) was used as received as the supporting electrolyte. Redox potentials were measured as halfway up the rising edge of the experimentally obtained steady-state voltammograms. $\Delta E$ was found to be 1.6 eV.

Fluorescence upconversion experiments were performed to measure the time-dependent ODRB fluorescence intensity. This is a direct experimental measurement of $\langle P_{ex}(t)\rangle$ for comparison with the theory. The upconversion experiments were performed using a frequency-doubled, mode-locked, Q-switched Nd:YLF laser pumping two dye lasers operating at 750 Hz. One dye laser was used for excitation of ODRB at the red-edge of its absorption spectrum (568 nm). The fluorescence was gathered and focused into an RDP crystal. The other dye laser provided an 850 nm upconverting pulse which was focused into the RDP crystal collinear with the fluorescence and polarized at the magic angle with respect to the excitation beam. When both wavelengths were present, sum-frequency light was generated which was proportional to the magnitude of the fluorescence during that time. The time dependence of the ODRB fluorescence was determined by scanning the arrival time of the excitation pulse at the sample relative to the fixed time of the upconverting pulse. The time-resolved sum-frequency light was detected by a dry ice cooled PMT connected to a gated integrator. The overall response of the system was 45 ps. The fluorescence yield measurements were performed by exciting with the same laser. In this case, the fluorescence passed through a polarizer set at the magic angle with respect to the excitation beam and was detected directly by a red-sensitive PMT. The measured signal for each sample with DMA was ratioed to one with only ODRB, and the ratio was corrected for differences in the ODRB optical density at the excitation wavelength.

## IV. Results

Figures 2−4 show fluorescence upconversion and fluorescence yield data for DTAB, TTAB, and CTAB, respectively, along with theoretical fits using eq 6. The fits are dashed lines. In many of the panels, the fits and the data are so nearly identical that they are indistinguishable. The center panels show the fluorescence yield numbers, with the circles being the data and crosses the theoretical fits using eq 7. Before discussing the fits quantitatively, which requires a specification of the distance-dependent rate coefficient, the results will be addressed qualitatively.

The three surfactants studied here differ only in the length of their alkyl chains ($C_{12}$ for DTAB, $C_{14}$ for TTAB, and $C_{16}$ for CTAB). We thus anticipate that differences in micelle radii will be the chief cause of differences in the transfer dynamics among the three micelles. In particular, given the similarity of the micelle structures, for the same donor−acceptor pair the distance-dependent rate coefficient, $k_f(\theta)$, would be expected to be very similar for the three micelles. (Additionally, the lateral diffusion coefficients would also be expected to be similar for the three micelles.) For a given (mean) number of DMA, denoted $N$, as the micelle radius increases, the likelihood of finding a donor near the ODRB decreases. Thus, for a fixed number of DMA, the amount of electron transfer should decrease as the micelle radius increases due a smaller fractional occupancy of the micelle surface. We define a "surface" packing fraction, $\eta$:

$$\eta = \frac{N\pi r_a^{\,2}}{4\pi R^2}$$

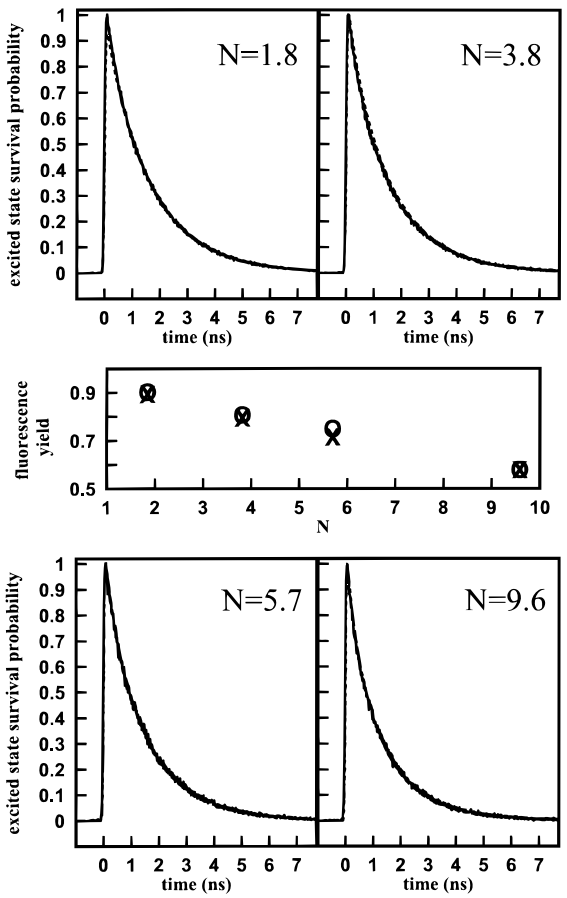


**Figure 2.** Fluorescence upconversion data (solid lines) and theoretical fits using eq 6 (dashed lines) for ODRB and four concentrations of DMA on DTAB. The center panel shows fluorescence yield data (circles) and the fits (crosses) from eq 7. The calculated yield numbers are within the error bars on the data. $N$ denotes the mean number of DMA per micelle. The theoretical fits shown are for parameters $J$ = 56 cm$^{-1}$, $\beta$ = 1.0 Å$^{-1}$, $D$ = 6.0 Å$^2$/ns, $\lambda_{\text{contact}}$ = 1.19 eV (see Discussion). Consistent fits to the data in all three micelles can be obtained only if the reorganization energy is assumed to vary among the three micelles.

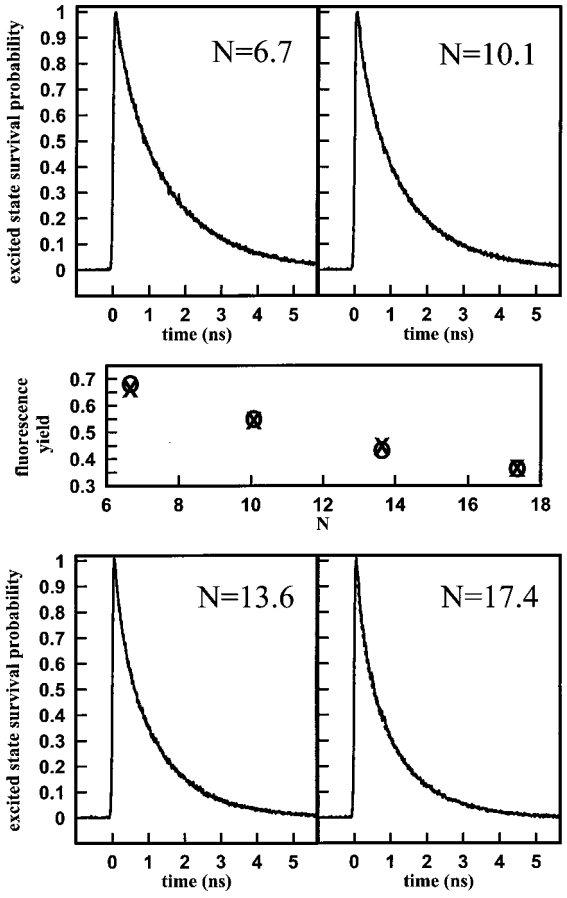


**Figure 3.** Fluorescence upconversion data (solid lines) and theoretical fits using eq 6 (dashed lines) for ODRB and four concentrations of DMA on TTAB. The fits are essentially indistinguishable from the data. The center panel shows fluorescence yield data (circles) and the fits (crosses) from eq 7. The theoretical fits shown are for parameters $J$ = 62 cm$^{-1}$, $\beta$ = 1.0 Å$^{-1}$, $D$ = 5.4 Å$^2$/ns, $\lambda_{\text{contact}}$ = 1.02 eV.

where $r_a$ is the DMA radius, $R$ the micelle radius, and $N$ the mean number of DMA per micelle. To the extent that the DMA and ODRB environments are the same in the three micelles, it might be anticipated that the electron-transfer kinetics would be very similar for the same $\eta$ on the three different micelles.

In Figure 5, we plot the electron-transfer contribution to the excited-state decay for each micelle for the same DMA packing fraction, $\eta$ = 8%. The curves are obtained by removing the fluorescence lifetime contribution, which is the same for each micelle. As can be seen, the decays are different for the three micelles, with the transfer fastest on CTAB, intermediate on TTAB, and slowest on DTAB. The packing fraction is not the sole determinate of the rate for electron transfer between the same donor/acceptor pair on similar micelles of different sizes. The influence of the size of the micelle on the dynamics of electron transfer is clear from the curves in Figure 5 and does not depend on a particular theoretical treatment. Furthermore, the differences in the curves shown in Figure 5 cannot be explained by error in the calculation of $\eta$ due, for example, to uncertainties in the micelle radii. This is best illustrated in Figure 6, which plots the fluorescence yield numbers (upper panel) and the 1/e points of the decay curves for the three micelles as a function of packing fraction. The lines in the figure serve as aids to the eye. For each micelle, there is a trend in which the electron-transfer rate increases with the DMA packing fraction. However, while the trend is approximately the same in the three micelles, the rates of electron transfer clearly differ, as is shown by the displaced slopes in Figure 6. To collapse the data points for all three micelles onto a single line, the error in the packing fraction would have to be on the order of 30%. An error of this magnitude would require the assumption that the radii of DTAB, TTAB, and CTAB are essentially identical. Such an assumption is not only counter-intuitive but contradicts detailed neutron and light scattering studies on these three micelles[30,31] as well as widely accepted theoretical models such as that of Tanford.[26] The increase in the electron-transfer kinetics with increasing surfactant chain length must be due to factors other than the DMA packing fraction.

## V. Discussion

To understand the factors contributing to the observed electron-transfer dynamics, we turn to the theory outlined above and developed in ref 1. The observable, $\langle P_{ex}(t)\rangle$, decays due to forward electron transfer at a rate determined by the number of acceptors, the lateral diffusion coefficient, and the distance-dependent rate coefficient. In section II, we avoided specifying a distance-dependent rate coefficient to preserve the generality of the theory. The ensemble-averaging procedure will work with any form of $k_f(\theta)$. The significance of the theory is that it properly performs the ensemble averages, with the lateral diffusion of the acceptor/donors appropriately included. The influence of the form of $k_f(\theta)$ on the data can be separated from

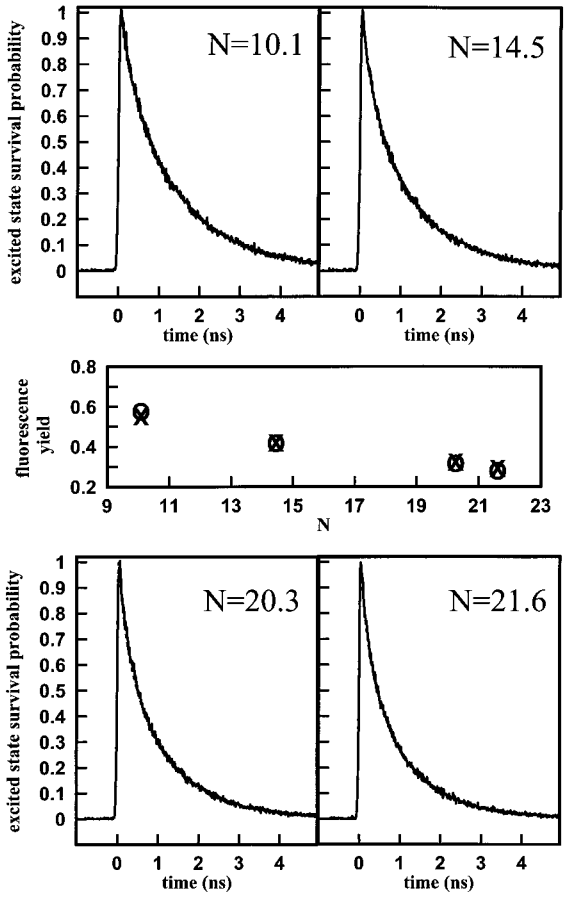


**Figure 4.** Fluorescence upconversion data (solid lines) and theoretical fits using eq 6 (dashed lines) for ODRB and four concentrations of DMA on CTAB. The fits are essentially indistinguishable from the data. The center panel shows fluorescence yield data (circles) and the fits (crosses) from eq 7. The theoretical fits shown are for parameters $J = 65$ cm$^{-1}$, $\beta = 1.0$ Å$^{-1}$, $D = 6.2$ Å$^2$/ns, $\lambda_{contact} = 0.93$ eV.

the effects of diffusion. Application of the theoretical methods presented here indicates that the difference in dynamics is due to real differences in $k_f(\theta)$ among the three micelles and not to differences in the DMA distribution or variations in the lateral diffusion coefficient. As demonstrated by the following analysis, the key is differences in the reorganization energies in the three micelles.

We choose a specific distance-dependent rate coefficient, $k_f(\theta)$. Most theories of electron transfer use a rate coefficient[21,22]

$$k_f(\theta) = \frac{2\pi}{\hbar}[H_{ab}(\theta)]^2 \mathrm{FCWD} \qquad (8)$$

We write the rate coefficient as a function of polar angle, $\theta$, rather than of the more familiar distance, $r$, for consistency with eqs 1−6. $r = 2R \sin(\theta/2)$. In eq 8, FCWD is the Franck−Condon weighted density of states and includes the free energy dependence and solvent reorganization. $H_{ab}(\theta)$ is the distance-dependent electronic coupling:

$$[H_{ab}(\theta)]^2 = J^2 \exp[-2R\beta(\sin(\theta/2) - \sin(\theta_c/2))] \qquad (9)$$

where $J$ denotes the electronic coupling at the donor−acceptor contact distance, $\theta_c$, and $\beta$ determines the distance dependence. The magnitude of the electronic coupling at the DMA/ODRB contact distance is not expected to vary significantly in the three micelles since this is mainly a property of the molecules themselves. $\beta$ is expected to have a magnitude of approximately 1 Å$^{-1}$ [32−36] and to be similar for the three micelles. In fitting

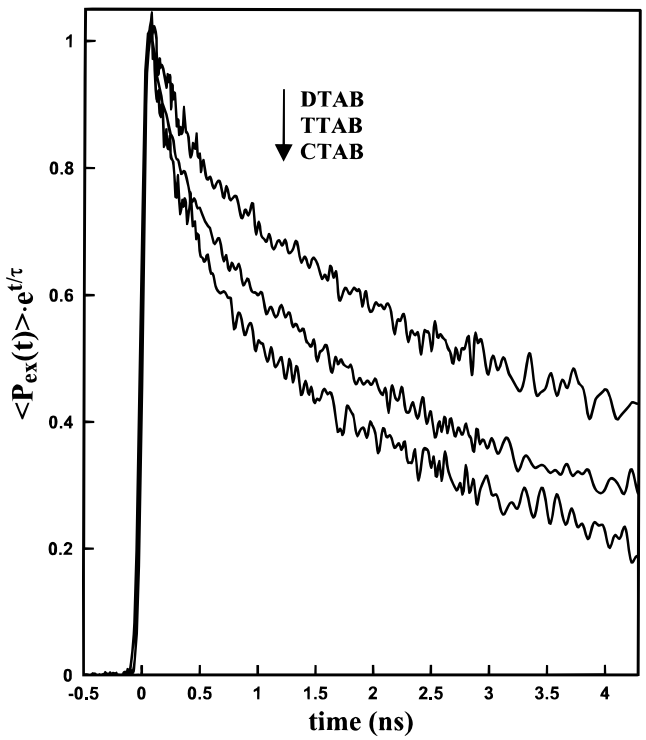


**Figure 5.** Excited-state survival probability $\langle P_{ex}(t)\rangle$ with the contribution from the fluorescence lifetime removed for samples with same DMA packing fraction (8%) on all three micelles. The slowest decay is DTAB, the intermediate TTAB, and the fastest CTAB. The rate of electron transfer is not identical for these three samples, although the physical properties and the DMA packing fraction are essentially identical.

the data, we used a classical form of the Marcus rate coefficient, expected to be good for electron-transfer reactions such as this one, occurring in the normal regime.

$$k_f(\theta) = \frac{2\pi}{\hbar}J^2 \exp[-2R\beta(\sin(\theta/2) - \sin(\theta_c/2))]\frac{1}{\sqrt{4\pi\lambda k_B T}}\exp\left[\frac{-(\Delta G_f + \lambda)^2}{4\lambda k_B T}\right] \qquad (10)$$

In eq 10, $\lambda$ is the solvent reorganization energy.[21,22,29] Marcus derived an analytical expression for the reorganization energy for spherical reagents in an isotropic dielectric continuum:[21]

$$\lambda = \frac{e^2}{2}\left(\frac{1}{\epsilon_{op}} - \frac{1}{\epsilon_s}\right)\left(\frac{1}{r_d} + \frac{1}{r_a} - \frac{1}{R\sin(\theta/2)}\right) \qquad (11)$$

where $\epsilon_{op}$ and $\epsilon_s$ are the optical and static dielectric constants, and $e$ is the fundamental charge. (The distance is specified in terms of $\theta$.) Equation 11 is not expected to apply precisely for the complex geometry at a micelle surface where the donor/acceptor sit at a hydrocarbon/water interface. For the moment though, we take $\lambda$ to be given by eq 11, acknowledging its deficiency for the current experimental situation, but preferring to keep a simple form of the distance-dependent reorganization energy in order to first make some key points about the experimental data. The important aspect to note is that we are initially choosing $\lambda$ to be the same for all three micelles, since $\epsilon_{op}$ and $\epsilon_s$ might be expected to be essentially identical for three such highly similar micelles. ($\epsilon_{op}$ and $\epsilon_s$ were taken to be those of water, 1.8 and 78, respectively. Variations in $\epsilon_s$ from 37 to 78, while consistent with the DMA fluorescence spectra, lead to negligible changes in $\lambda$.)

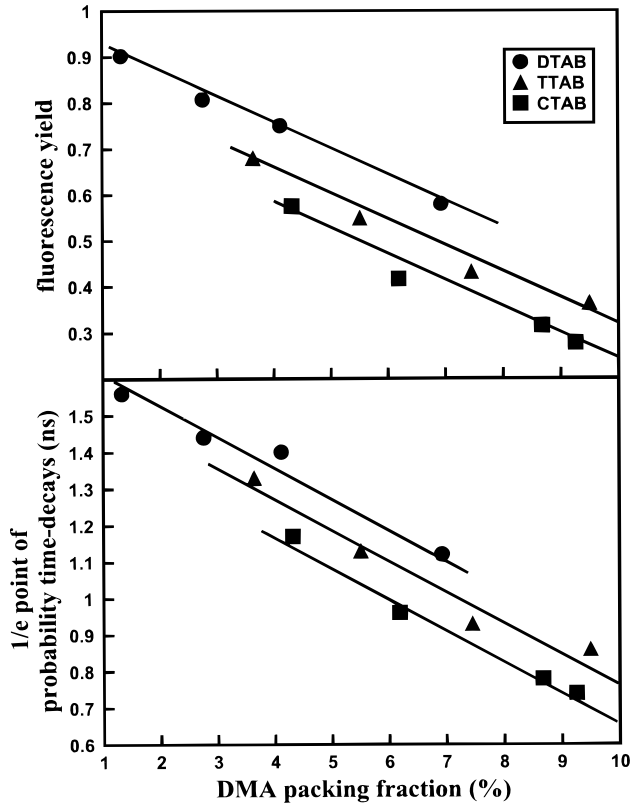


**Figure 6.** Plots of fluorescence yield and 1/e point of decays vs DMA packing fraction for all three micelles. Lines are guides to the eye. The plot of 1/e points is not intended to imply that the decays are exponential. Clearly, the amount of transfer occurring in the three micelles is not dependent solely on DMA packing fraction.

Using eq 10 and eqs 1−6 to fit the data requires knowledge of $J$ and $\beta$ as well as the lateral diffusion constant $D$. Although all three could be treated as adjustable parameters, such a fitting procedure is not particularly useful. Instead, we initially chose $\beta = 1.0$ Å$^{-1}$. This value is consistent with measurements of $\beta$ from intramolecular and intermolecular electron-transfer experiments which generally find $\beta$ centered in the range 0.8−1.4.[32−36] We will discuss the dependence of the fits on the choice of the $\beta$ value below.

In generating the fits to the data in Figures 2−4, we initially treated $J$ and $D$ as adjustable parameters. For any given $J$ and $D$ pair, eq 6 must predict the time decay profiles for all four concentrations on a single micelle, while eq 7 must simultaneously give good agreement with the experimental fluorescence yield data. With two adjustable parameters used to fit four time-dependent curves and four yield numbers, we obtain unique fits. The quality of fits was ascertained by a $\chi^2$ value assigned by a fitting routine based on the downhill simplex method.[37,38] The $\chi^2$ value for a given $J$ and $D$ pair consisted of contributions from all four time decays (each weighted equally) and from the fluorescence yield data (given the weight of one full time decay.)

The first result to be noticed from Figures 2−4 is that the quality of fits is excellent for all three micelles. The lowest concentration DTAB curve shows an early time discrepancy, but otherwise the agreement is extremely good; the fits are almost indistinguishable from the data. The second result from the theoretical fits is that the $J$ values required to fit the data differ substantially among the micelles. From fixing $\beta$ at 1.0 and fitting $J$ and $D$, the best fits to the data are $J = 50$ cm$^{-1}$, $D = 5$ Å$^2$/ns for DTAB, $J = 100$ cm$^{-1}$, $D = 6$ Å$^2$/ns for TTAB, and $J = 190$ cm$^{-1}$, $D = 7$ Å$^2$/ns for CTAB. In the treatment thus far, the other parameters in eq 10 have been assumed to be invariant. No matter what choice we make for $\beta$ or $\lambda$, provided only that they are the same for all three micelles, the $J$ values needed to fit the data increase dramatically with increasing surfactant chain length.

As Figures 5 and 6 show, independent of any theoretical argument, the amount of electron transfer increases as the micelle is changed from DTAB to TTAB to CTAB for a constant DMA packing fraction. To yield fits to the data and reproduce this trend, the theory gives $J$ values that increase substantially with the surfactant chain length. Although the diffusion coefficients also increase with micelle size, this effect is not significant enough to account for the data without also assuming large variations in $J$. Since $J$ is the magnitude of the ODRB/DMA electronic coupling at the contact distance, there is no reason to expect that this parameter should change significantly as the micelle is altered. Instead, other differences, not yet allowed to vary with the size of the micelle, may be responsible for the faster kinetics observed for larger micelles.

One possibility is that the DMA is not solubilized at the micelle surface as assumed. Although the NMR results of Eriksson and Gillberg[18] indicate that all the DMA should be located near the surfactant headgroup, we must consider the possibility that some fraction of DMA is dissolved elsewhere. We have already discussed the fluorescence evidence against DMA localization in the micelle core. There remains the possibility that a small amount of DMA is freely dissolved in the water. Calculations show that DMA concentrations such as those used here (<6 mM) result in no observable electron transfer within the ODRB lifetime if the DMA is distributed in an isotropic liquid. However, let us assume that, while most DMA is micelle-bound, some fraction remains free in the water. Further, we could assume that the fraction of free DMA depends on the particular micelle and is greatest for DTAB and smallest for CTAB. The primary effect that the free DMA would have on the electron-transfer dynamics would be through reducing the mean number of DMA at the micelle surface, $N$. This reduction would be greatest for DTAB, so that in generating fits to the electron-transfer data on DTAB, we would be using values of $N$ that were too high. To compensate for an error of this type, too small $J$ values would result from fits to the DTAB data. However, while a hypothesis of this type might seem reasonable, it cannot explain the trends in the data. If we attempt to fit the transfer data on DTAB with the mean number of DMA at the micelle surface reduced by up to 30%, $D$ increases some, but $J$ does not increase much above 50 cm$^{-1}$, which is still much smaller than the $J$ values for TTAB and CTAB. If $N$ is reduced by more than about 30%, it becomes impossible to fit the data on DTAB. Furthermore, spectroscopic evidence rules out a large fraction of the DMA being free in the water. The absorption spectrum of DMA in water is significantly different from that in DTAB. The difference is large enough that any significant amount of DMA in water would appear as a separate peak or at least a large shoulder on the DMA in DTAB spectrum. These is no sign of such a peak or shoulder in the DMA in DTAB spectrum. Thus, variations in DMA packing fraction on the micelle surfaces produced by DMA free in the water cannot explain the observed increase in transfer rate with increasing micelle radius.

A second possibility is that, while DMA is localized near the micelle surfaces, errors in calculating the micelle radii are responsible for the discrepancy in $J$ values. The radii values used (see Table 1) were calculated from the Tanford equations for DMA located just outside the hydrocarbon core. It is possible that these estimates are too small and that the DMA is

located further from the center of the micelle, near the counterions for example. In such a case, the radii of all three micelles would be increased from 16.7, 19.2, and 21.7 Å to 20.0, 22.5, and 25.0 Å for DTAB, TTAB, and CTAB, respectively. These larger numbers are consistent with the hydrodynamic radii measured by light scattering experiments.[30] Larger radii would mean a smaller DMA surface packing fraction and thus a reduced probability of finding a donor and acceptor near one another. The $J$ values would then need to be correspondingly increased to account for the same amount of electron transfer. When we increase the radii of the three micelles to 20.0, 22.5, and 25.0 Å, the $J$ values from the fits do indeed increase. However, the spread in $J$ values from DTAB to TTAB to CTAB is not narrowed. Using radii of 16.7, 19.2, and 21.7 Å gives $J$ values of 50, 100, and 190 $cm^{-1}$ for DTAB, TTAB, and CTAB, respectively. Using the larger radii of 20.0, 22.5, and 25.0 Å gives $J$ values of 62, 174, and 355 $cm^{-1}$. For the distance-dependent rate coefficient, $k_f(\theta)$, to be the same for all three micelles, we would have to assume that the micelle radii for DTAB, TTAB, and CTAB are *essentially identical*. Such an assumption is inconsistent with neutron and light scattering data and with theory. Even if there is some uncertainty about where the DMA is solubilized, an error in the input location of the DMA into the calculations cannot account for the observed trend with micelle size.

Recently, work from this laboratory on intermolecular electron transfer in liquids has demonstrated the importance of including certain solvent structural effects in the theory.[39,40] In particular, the solvent radial distribution function, $g(r)$, and distance-dependent diffusion coefficient, $D(r)$, affect both the spatial averaging and the diffusive motion. In principle, both these effects should be present at a micelle surface. However, we know of no theoretical formalism for calculating the magnitude and range of $g(r)$ or $D(r)$ on spherical surfaces. Nonetheless, given the demonstrated importance of solvent effects in isotropic liquid systems,[39,40] we need to consider at least approximate expressions to determine if variations in $g(r)$ or $D(r)$ among the micelles might be responsible for the observed trend in transfer rates. To a first approximation, the formalisms used in isotropic liquid systems may give at least qualitatively correct results near the micelle surface. A real micelle does not possess an ideal two-dimensional surface; the micelle−water boundary is not rigidly defined, and acceptor/donors may sink slightly into or rise slightly above the micelle surface. Thus, on a molecular scale, the region surrounding a given donor/acceptor is actually three-dimensional, with water penetrating into the micelle headgroup region.[41] Given the level of approximation involved in applying three-dimensional formalisms to micelle surfaces, we made no attempt to perform detailed calculations accounting for the various components (water, headgroups, counterions, etc.) present at the micelle surface. Instead, we have used hard sphere $g(r)$ calculations with a variety of packing fractions and hard sphere diameters. (See ref 39 for details on how to incorporate these effects into a theory of photoinduced intermolecular electron transfer.) We have also used radial distribution functions reported from molecular dynamics simulations of micelle systems.[42] For the hydrodynamic effect, we tested both stick and slip boundary conditions[43] and adjusted the range of the effect to account for various possible solvent sizes. No matter what form of $g(r)$ or $D(r)$ we used within a reasonable range, even if we allowed the forms to differ wildly from micelle to micelle, we were unable to fit the data with the same $J$ value for all three micelles. Inclusion of $g(r)$ and $D(r)$ led to a value of $J$ decreased by up to 50% for each micelle, primarily because the local concentration of DMA about the ODRB increased due to the first peak in the radial distribution function. However, the decrease in $J$ value occurred for all three micelles, and even with different forms of $g(r)$ and $D(r)$ for the micelles, DTAB consistently had a $J$ value much smaller than the other two micelles. Thus, solvent structural effects are insufficient to account for the observed rapid increase in the amount of electron transfer as the surfactant chain length increases.

Neither error in the concentration of DMA at the micelle surface, nor uncertainty in the micelle radii, nor neglect of $g(r)$ and $D(r)$ can account for the fact that, for a given DMA packing fraction, electron transfer is fastest in CTAB, intermediate in TTAB, and slowest in DTAB. The qualitative conclusion is that the electron-transfer rate coefficient, $k_f(\theta)$, must actually increase with surfactant chain length. Fitting the data with only $J$ and $D$ treated as the adjustable parameters, it was impossible to generate good fits to the data in all three micelles with the same $J$ but different $D$ values. Since $J$ (the magnitude of the electronic coupling at contact) seems the one parameter most likely to remain nearly constant as the micelle is changed, we now consider the other parameters determining the Marcus rate equation ($\beta$, $\Delta G$, $\lambda$, $\epsilon_{op}$, and $\epsilon_s$). Any of these might reasonably be expected to vary somewhat from micelle to micelle.

If $J$ is assumed to be constant for electron transfer in the three micelles, $D$ is treated as a fitting parameter, and $\beta$ is allowed to vary from micelle to micelle within the wide range of 0.7−1.6 $Å^{-1}$, good fits to the data in all three micelles cannot be obtained for any consistent $J$ value.

As discussed previously, the free energy of the reaction, $\Delta G$, was taken from cyclic voltammetry measurements in acetonitrile. The change in $\Delta G$ at contact from one solvent to another can be calculated using the Born equation:[44]

$$\Delta(\Delta G) = \frac{e^2}{r}\left(\frac{1}{\epsilon_1} - \frac{1}{\epsilon_2}\right)$$

where $e$ is the fundamental charge, $r$ is the average molecular radius (average of donor and acceptor), and $\epsilon_1$ and $\epsilon_2$ are the static dielectric constants of the original and final solvents, respectively. From this equation, the local static dielectric constant on the three micelles would have to vary from 27 to 78 in order to account for a 0.1 eV change in $\Delta G$. Such wide variation in the static dielectric constant is not consistent with the DMA fluorescence spectra. Furthermore, even if $\Delta G$ is assumed to vary by 0.1 eV, the $J$ values for the three micelles still increase sharply with surfactant chain length.

Thus far, we have assumed that the solvent reorganization energy, $\lambda$, is the same for the three micelles and is given by eq 11. Equation 11 was derived for spherical reagents in an isotropic continuum. This expression will not be valid at the surface of a micelle. A rigorous calculation of $\lambda$ for a very simple model of a micelle requires solving the Poisson equation for the donor and acceptor located at the surface of a sphere composed of hydrocarbon and surrounded by water.[45−49] More realistically, the donors and acceptors are located in a spherical shell of ∼4 Å thickness. Inside the 4 Å shell are the micelle headgroups, some hydrocarbon, and substantial amounts of water with the counterions nearby, creating a dielectric medium with properties somewhere between those found on either side of the shell, i.e. water on one side, hydrocarbon on the other. (If the counterions are important, the Poisson−Boltzmann equation must be solved.) The reorganization energy may vary significantly as the size of the hydrocarbon core changes. Performing a detailed calculation of the reorganization energy for a realistic description of a micelle is not a trivial problem,

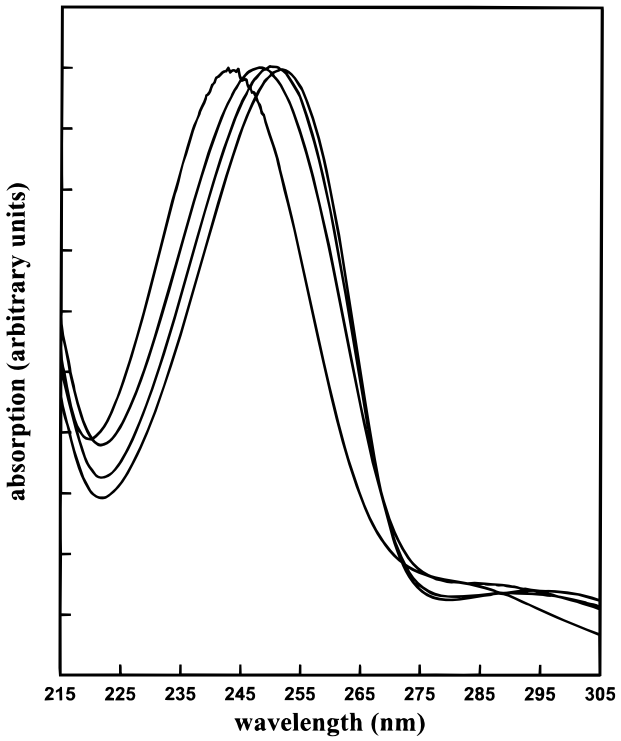


**Figure 7.** Absorption spectra of DMA in water (leftmost spectrum) and in DTAB, TTAB, and CTAB aqueous micelle solutions (from left to right). The spectra are scaled to match peak heights. The 250 nm peak shifts by 2 nm from one micelle to the next. Spectra were taken against a reference consisting of water or the appropriate aqueous micelle solution containing no DMA.

and work is in progress to perform such calculations, beginning with the simplest model.

To understand the experimental data presented here, we give a qualitative argument based on evidence that the local DMA environment varies from micelle to micelle. Figure 7 shows the absorption spectra of DMA in the three aqueous micelle solutions and in water. The absorption spectrum of DMA in water is shifted several nanometers to the blue. As can be seen from the figure, the DMA environment varies in a consistent fashion as the micelle is changed from DTAB to TTAB to CTAB. The spectral shifts demonstrate that there are changes in the local optical and static dielectric constants. Although formalisms based on Onsager's theory of dielectrics could be utilized to quantify the variations in dielectric constants from shifts in the absorption spectra,[50] these formalisms are derived assuming an isotropic continuum and are insufficient for micelle surfaces. Of the three micelles, the DMA absorption spectrum in DTAB is closest to that of DMA in water. This result is consistent with recent neutron scattering data on these three micelles which indicate that the extent of water penetration into the micelle decreases with increasing alkyl chain length.[31] Greater water penetration (a more polar environment) is expected to lead to a larger value of the solvent reorganization energy, $\lambda$. The absorption spectra are consistent with an increase in $\lambda$ as the surfactant chain length decreases.

To ascertain whether differences in $\lambda$ could account for the observed acceleration of the electron transfer as the micelle size increases, we allowed $\lambda$ to vary from DTAB to TTAB to CTAB. Although eq 11 is valid only in an isotropic dielectric continuum, we note that reasonable variations in the optic and static dielectric constants could lead to a 15% change in $\lambda$. Basically, we are assuming for this preliminary analysis that the form of the distance dependence is the same as that given by eq 11, but the magnitude of the prefactor varies with micelle size. If $\lambda$ is assumed to increase as the micelle radius decreases (due to an increase in the extent of hydration for example), excellent fits to the data in all three micelles can be obtained. The best fits to the data are for the parameters $J = 56$, 62, and 65 $cm^{-1}$ and $\lambda_{contact} = 1.19$, 1.02, and 0.93 eV for DTAB, TTAB, and CTAB, respectively, with a diffusion constant of $6 \pm 1$ $Å^2$/ns and $\beta = 1.0$ $Å^{-1}$ for all three micelles. The differences in these $J$ values are insignificant within experimental error, and in fact, the data could all be fit with the same $J$ with virtually no change in the quality of the fits. These are the very high quality fits shown in Figures 2−4, assuming $\lambda(\theta) = \lambda_{contact}[1/r_d + 1/r_a - 1/R \sin(\theta/2)]$. The variation in $\lambda$ is not unreasonable, and the $\lambda$ value in DTAB is approaching that which would occur for DMA and ODRB dissolved in pure water. The $\lambda$ values and trends are consistent with the neutron scattering data of Berr, Jones, and Johnson which indicate that the amount of water penetration is greatest for DTAB, least for CTAB, and intermediate for TTAB. The trend in $\lambda$ is also consistent with the absorption spectra.

The values given in the preceding paragraph should not be regarded as exact, since at this point $\lambda$ is not calculated rigorously, and $J$, $\beta$, and $D$ will vary somewhat with the precise choice of $\lambda$. Additionally, $g(r)$ and $D(r)$ are not included in these fits, and they may have some affect on the calculated dynamics. The important fact is that essentially perfect agreement with the data is obtained with J, $\beta$, and $D$ the same for the three micelle systems. The results indicate that the reorganization energy differs significantly even for similar micelles and that this difference in $\lambda$ can lead to a pronounced effect on the electron-transfer dynamics.

## VI. Concluding Remarks

We have analyzed photoinduced electron transfer between DMA and ODRB on the surfaces of three alkyltrimethylammonium bromide micelles: DTAB, TTAB, and CTAB. Direct examination of the data indicates that the amount of forward electron transfer increases with micelle radius for the same DMA packing fraction. From theoretical and physical arguments, we expect that, for micelles differing only in their radii, the amount of electron transfer should be determined by the density of DMA on the micelle surface. In fact, this result is not observed.

To understand why electron transfer on CTAB would be faster than on TTAB, which in turn would be faster than on DTAB, we need to separate the effects of diffusion, micelle structure, and the distance-dependent electron-transfer rate. Electron transfer at micelle surfaces is a complicated problem, and determining the influence of the various factors on the transfer dynamics requires a detailed theoretical model. The theoretical methods presented in ref 1 take into account the competition between the various donors, any one of which may quench the ODRB fluorescence. The theory also includes lateral diffusion of the acceptor/donors over the micelle surfaces and rigorously performs the ensemble averaging to give an exact description of electron-transfer dynamics for the model considered. We believe this model is a reasonable approximation to dynamics on real micelle surfaces.

Application of the theory to the experimental data presented here enables the different contributions to the electron-transfer dynamics to be understood. From fits to the experimental data, we have determined that the differences in the electron-transfer kinetics in the three micelles stem from real differences in the distance-dependent rate coefficients, and not from differences in the DMA distributions or the lateral diffusion coefficients. Electron-transfer rates are fastest on CTAB, intermediate on TTAB, and slowest on DTAB because the solvent reorganization

energy increases as the surfactant chain length decreases. This result may be due to increased water penetration into the smaller micelles, consistent with recent neutron scattering results. Contributions to the reorganization energy arising from geometric factors, e.g., the changing size of the hydrocarbon core, may also be important.

**Acknowledgment.** We would like to thank Prof. William Gelbart, Department of Chemistry, the University of California at Los Angeles, for many very helpful discussions pertaining to the structure and dynamics of micelles. We would also like to thank Dr. Marshall Newton, Brookhaven National Laboratory, for very informative conversations pertaining to the calculation of reorganization energies in micelles. This work was supported by the Department of Energy, Office of Basic Energy Sciences (Grant DE-FG03-84ER13251). H.L.T. thanks the Office of Naval Research for a graduate fellowship.

## References and Notes

(1) Weidemaier, K.; Fayer, M. D. *J. Phys. Chem.* **1996**, *100*, 3767.
(2) Barzykin, A. V.; Tachiya, M. *Heterog. Chem. Rev.* **1996**, *3*, 105.
(3) Grätzel, M. In *Photoinduced Electron Transfer. Part D*; Fox, M. A., Chanon, M., Eds.; Elsevier: New York, 1988; p 394.
(4) Fox, M. A. In *Topics in Current Chemistry*; Mattay, J., Ed.; Springer-Verlag: Berlin, 1991; Vol. 159, pp 67−101.
(5) Thomas, J. K. *Acc. Chem. Res* **1977**, *10*, 133.
(6) Waka, Y.; Hamamoto, K.; Mataga, N. *Chem. Phys. Lett.* **1979**, *62*, 364.
(7) Sano, H.; Tachiya, M. *J. Chem. Phys.* **1981**, *75*, 2870.
(8) Grätzel, M.; Thomas, J. K. *J. Phys. Chem.* **1974**, *78*, 2248.
(9) Rothenberger, G.; Gratzel, M. *Chem. Phys. Lett.* **1989**, *154*, 165.
(10) Hammarström, L.; Berglund, H.; Almgren, M. *J. Phys. Chem.* **1994**, *98*, 9588.
(11) Lerebours, B.; Chevalier, Y.; Pileni, M. P. *Chem. Phys. Lett.* **1985**, *117*, 89.
(12) Nakagaki, M.; Komatsu, H.; Tanaka, H.; Handa, T. *Bull. Chem. Soc. Jpn.* **1986**, *59*, 3007.
(13) Hubig, S. M. *J. Lumin.* **1991**, *47*, 137.
(14) Nery, H.; Soderman, O.; Canet, D.; Walderhaug, H.; Lindman, B. *J. Phys. Chem.* **1986**, *90*, 5802.
(15) Walderhaug, H.; Soderman, O.; Stilbs, P. *J. Phys. Chem.* **1984**, *88*, 1655.
(16) Eriksson, P.-O.; Khan, A.; Lindblom, G. *J. Phys. Chem.* **1982**, *86*, 387.
(17) Lindman, B. In *Surfactants*; Tadros, T. F., Ed.; Academic Press: Inc.: Orlando, 1984; pp 83−110.
(18) Eriksson, J. C.; Gillberg, G. *Acta Chem. Scand.* **1966**, *20*, 2019.
(19) Grätzel, M.; Kalyanasundaram, K.; Thomas, J. K. *J. Am. Chem. Soc.* **1974**, *96*, 7869.
(20) Weidemaier, K.; Fayer, M. D. *J. Chem. Phys.* **1995**, *102*, 3820.
(21) Marcus, R. A. *J. Chem. Phys.* **1956**, *24*, 966.
(22) Marcus, R. A. *Annu. Rev. Phys. Chem.* **1964**, *15*, 155.
(23) Reiss-Husson, F.; Luzzati, V. *J. Phys. Chem.* **1964**, *68*, 3504.
(24) Lin, Z.; Cai, J. J.; Scriven, L. E.; Davis, H. T. *J. Phys. Chem.* **1994**, *98*, 5984.
(25) Vinson, P. K.; Bellare, J. R.; Davis, H. T.; Miller, W. G.; Scriven, L. E. *J. Colloid Interface Sci.* **1991**, *142*, 74.
(26) Tanford, C. *J. Phys. Chem.* **1972**, *76*, 3020.
(27) Ediger, M. D.; Domingue, R. P.; Fayer, M. D. *J. Chem. Phys.* **1984**, *80*, 1246.
(28) Rehm, D.; Weller, A. *Isr. J. Chem.* **1970**, *8*, 259.
(29) Bolton, J. R.; Archer, M. D. In *Electron Transfer in Inorganic, Organic, and Biological Systems*; Bolton, J. R., Mataga, N., McLendon, G., Eds.; The American Chemical Society: Washington, 1991; p 7.
(30) Dorshow, R.; Briggs, J.; Bunton, C. A.; Nicoli, D. F. *J. Phys. Chem.* **1982**, *86*, 2388.
(31) Berr, S.; Jones, R. R. M.; Johnson, J. S. *J. Phys. Chem.* **1992**, *96*, 5611.
(32) Closs, G. L.; Miller, J. R. *Science* **1988**, *240*, 440.
(33) Gray, H. B.; Winkler, J. R. *Annu. Rev. Biochem.* **1996**, *65*, 537.
(34) Miller, J. R.; Beitz, J. V.; Huddleston, R. K. *J. Am. Chem. Soc.* **1984**, *106*, 5057.
(35) Marcus, R. A.; Sutin, N. *Biochim. Biophys. Acta* **1985**, *811*, 265.
(36) Guarr, T.; McLendon, G. *Coord. Chem. Rev.* **1985**, *68*, 1.
(37) Press: W. H.; Flannery, B. P.; Teukolsky, S. A.; Vetterling, W. T. *Numerical Recipes in C*; Cambridge University Press: Cambridge, 1988.
(38) Nelder, J. A.; Mead, R. *Comput. J.* **1965**, *7*, 308.
(39) Swallen, S. F.; Weidemaier, K.; Fayer, M. D. *J. Chem. Phys.* **1996**, *104*, 2976.
(40) Weidemaier, K.; Tavernier, H. L.; Swallen, S. F.; Fayer, M. D. *J. Phys. Chem. A* **1997**, *101*, 1887.
(41) Chandler, D. Personal communication.
(42) Laaksonen, L.; Rosenholm, J. B. *Chem. Phys. Lett.* **1993**, *216*, 429.
(43) Rice, S. A. *Diffusion-Limited Reactions*; Elsevier: Amsterdam, 1985.
(44) Weller, A. *Z. Phys. Chem. NF* **1982**, *133*, 93.
(45) Zaloj, V.; Agmon, N. *Chem. Phys. Lett.* **1997**, *270*, 476.
(46) Kharkats, Y. I.; Krishtalik, L. I. *J. Theor. Biol.* **1985**, *112*, 221.
(47) Krishtalik, L. I. *J. Theor. Biol.* **1985**, *116*, 201.
(48) Dilonardo, M.; Maestro, M. *Chem. Phys. Lett.* **1991**, *180*, 353.
(49) Newton, M. D. Personal Communication.
(50) Birks, J. B. *Photophysics of Aromatic Molecules*; Wiley-Interscience: London, 1970.
(51) van Os, N. M.; Haak, J. R.; Rupert, L. A. M. *Physico-Chemical Properties of Selected Anionic, Cationic, and Nonionic Surfactants*; Elsevier: Amsterdam, 1993.